International Journal of Solids and Structures 241 (2022) 111497

Contents lists available at ScienceDirect

International Journal of Solids and Structures

journal homepage: www.elsevier.com/locate/ijsolstr

Three-dimensional non-planar crack growth analysis using enriched finite elements

Emre Kurt [a], Oğuzhan Demir [b,*], Ali O. Ayhan [a]

[a] Department of Mechanical Engineering, Sakarya University, 54050 Sakarya, Turkey
[b] Department of Mechanical Engineering, Bilecik Seyh Edebali University, 11210 Bilecik, Turkey

ARTICLE INFO

Keywords:
Computational fatigue crack propagation
Mixed Mode-I/II/III
Non-planar crack growth
Three-dimensional crack growth criterion

ABSTRACT

The paper presents computational mixed mode non-planar fatigue crack growth analyses using Fracture and Crack Propagation Analysis System (FCPAS), which employs enriched crack tip finite elements to calculate the mixed mode stress intensity factors (SIFs) and utilizes from other sub-modules to predict the evolving crack growth trajectories and the resulting fatigue crack growth lives. Numerical applications on different problems selected from the literature; a hollow shaft, an H-shaped specimen and cylindrical rods containing cracks with different initial orientations and sizes and subjected to different fatigue loading types are presented. Comparisons of results from the numerical analyses with the corresponding data from the literature agree well in terms of computed SIFs, predicted evolving crack paths and crack propagation lives.

1. Introduction

In 1963, Paris and Erdoğan (Paris and Erdogan, 1963) introduced the well known and still-widely used relationship between the fatigue crack growth rate and the elastic stress intensity factor (SIF). Tanaka (Tanaka, 1974) modified the Paris and Erdogan's law for mixed mode-I/II fatigue crack growth problems in 1970s and developed an empirical equivalent stress intensity factor range (ΔK_{eq}) criterion that encompasses the effects of mode-I and II SIFs. In the case of a three-dimensional mixed mode fracture problem, ΔK_{eq} expresses the superposition of mode-I, -II and -III SIFs. Non-planar crack trajectory and propagation life under 3-D fatigue loads depend on the computed stress intensity factors (SIFs) along the crack front. The selection of a convenient ΔK_{eq} model plays a significant role on prediction of fatigue crack propagation surface and life. ΔK_{eq} values and crack deflection angles (θ) along the crack front need to be computed by using separate models and for each crack front node on the respective propagation step during crack growth modeling. There have been a few crack growth criteria proposed for three-dimensional mixed mode-I/II/III problems. Pook (Pook, 1980, 1985), Sih (Sih, 1991); Schöllmann et al. (Schöllmann et al., 2002), Richard et al. (Richard et al., 2005; Richard, 2001) and Demir et al. (Demir et al., 2017; Demir et al., 2019) developed fracture criteria to predict crack kinking and/or twisting angles and ΔK_{eq} for 3-D mixed mode-I/II/III crack growth problems. Moreover, empirical ΔK_{eq} equations also exist in the literature proposed by Tanaka (Tanaka, 1974) and Kikuchi et al. (Kikuchi et al., 2012).

In computational crack growth analysis, in addition to the above-mentioned criteria, numerical modeling and the type of used numerical method are also key factors for predicted incrementally growing crack shape and corresponding propagation lives. Numerical investigations on fatigue crack growth in engineering structures became very common using the finite element method on linear elastic fracture mechanics (LEFM) problems. Modeling and analysis of non-planar crack propagation are much more complicated due to curvilinear form of incremental cracks compared to mode-I problems, in which crack propagates in its initial plane. Necessary pre-and post-process interventions for some non-planar crack growth problems may require significant amount of effort and might be much more time-consuming than the computational solution time of the analysis (Demir and Ayhan, 2018; Nart and Ayhan, 2011).

Over the past two decades, numerous studies have been conducted to develop customized tools and methods for three-dimensional fracture and crack growth analysis using numerical techniques. Although the initial studies were conducted using the boundary elements technique (Mi and Aliabadi, 1994; Neves et al., 1997), most studies in the literature focused on analyses performed using the finite element method. Moreover, various hybrid numerical techniques such as finite element/dual boundary element method, which eliminates their disadvantages when

* Corresponding author.
E-mail address: oguzhan.demir@bilecik.edu.tr (O. Demir).

https://doi.org/10.1016/j.ijsolstr.2022.111497
Received 7 September 2021; Received in revised form 1 February 2022; Accepted 6 February 2022
Available online 10 February 2022

used separately while offering advantages with their integrated use, have also been reported in the literature (Citarella et al., 2016; Citarella et al., 2018; Giannella et al., 2017; Giannella et al., 2019). ADAPCRACK3D (Schöllmann et al., 2003), ZENCRACK (Hou et al., 2001; ZENCRACK user manual, 1999), FRANC3D (Carter et al., 1995; Carter et al., 2000) and BEASY (Neves et al., 1997; Curtin et al., 1999) are some of the most common programs that can perform three-dimensional fracture and crack growth analysis using these methods. FRANC3D software was developed to be used initially with the boundary element method in the late 1980's, and currently supports three commercial finite element based codes; ABAQUS, ANSYS and NASTRAN. Other software interfacing with these three commercial codes are ZENCRACK and BEASY. ZENCRACK generates cracked meshes automatically from uncracked finite element models to calculate fracture parameters, such as energy release rate and stress intensity factors. BEASY, which is based on boundary element method is capable of performing automatic crack growth simulations under complex fatigue loads and is integrated with finite element analysis systems. ADAPCRACK3D software uses the finite element method to perform crack growth analysis automatically and works in conjunction with ABAQUS. The enriched finite element method is also a preferred method from the perspectives of not needing pre- and post-process interventions, as it does not require a particular mesh structure near the crack front and additional treatments after solution of the finite element analysis. Ayhan and Nied (Ayhan and Nied, 1998; Ayhan and Nied, 2002) introduced a stand-alone general-purpose finite element-based 3-D fracture analysis program, FRAC3D, which is part of Fracture and Crack Propagation Analysis System (FCPAS). FRAC3D solver employs enriched crack tip finite elements to compute SIFs. Until now, there have been successfully performed studies by FRAC3D for interface cracks (Ayhan et al., 2007), mode-I (Ayhan and Nied, 2002) and mixed mode cracks (Ayhan, 2004; Ayhan, 2007) in homogeneous materials and cracks in functionally graded materials (Ayhan, 2007; Ayhan, 2009).

In this study, computational fatigue crack propagation analyses of mixed mode-I/II/III problems selected from the literature are carried out using FRAC3D. The numerical applications considered in the study are; a cylindrical rod containing an inclined initial crack under tension fatigue load (Okada et al., 2013), a hollow shaft with an initial semi-elliptical crack subject to bending fatigue load (Citarella et al., 2018) and H-shaped specimen with a semi-circular crack under tension fatigue load (Grasso et al., 2018).

2. Procedure for simulation of 3-D non-planar crack growth

In this subsection, process steps of fatigue crack propagation analysis procedure are provided. The finite element models containing initial and evolving cracks are generated using ANSYS^{TM} (ANSYS, 2009). The element, node lists connected to crack front and the whole model, and load, displacement lists belonging to whole model are taken from ANSYS. Those data are, then, converted and imported into FRAC3D solver to carry out fracture analysis. FRAC3D employs enriched crack tip elements to calculate SIFs, which are computed simultaneously together with nodal displacements without any post-processing intervention, along the crack front. The elements surrounding the whole crack front are named as the enriched finite elements and those elements between the enriched and regular finite elements are defined as transition elements. A representative view of a 20-noded hexahedral enriched finite element on the crack front is given in Fig. 1. The nodal displacements and SIFs along the crack front can be calculated simultaneously, since the unknown nodal SIFs are included into finite element formulation of the enriched elements in addition to shape functions and nodal displacements. As an example, the enriched element's x-direction displacement, u, is given by Eq. (1). Further details related to other displacement components, strains and numerical integration of enriched elements can be found in (Ayhan and Nied, 1998; Ayhan and Nied, 2002).

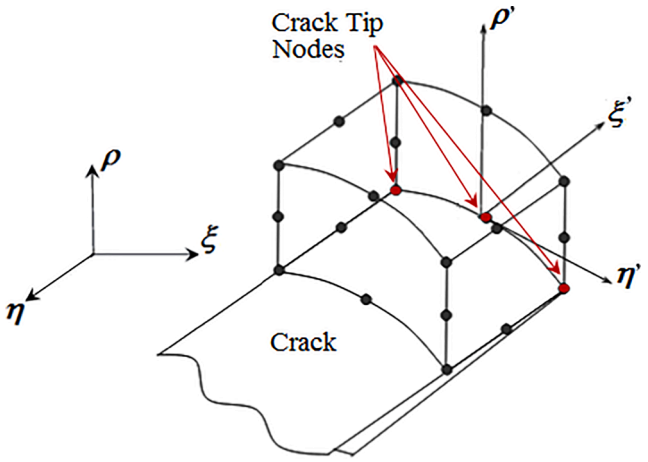

Fig. 1. A 20-noded hexahedral enriched finite element touching the crack front and located on a crack surface (Ayhan, 2004).

$$
\begin{aligned}
u(\xi,\eta,\rho) = {} & \sum_{j=1}^{m} N_j(\xi,\eta,\rho)u_j + Z_0(\xi,\eta,\rho)\left(f_u(\xi,\eta,\rho) - \sum_{j=1}^{m} N_j(\xi,\eta,\rho)f_{uj}\right)\left(\sum_{i=1}^{ntip} N_i(\Gamma)K_I^i\right) \\
& + Z_0(\xi,\eta,\rho)\left(g_u(\xi,\eta,\rho) - \sum_{j=1}^{m} N_j(\xi,\eta,\rho)g_{uj}\right)\left(\sum_{i=1}^{ntip} N_i(\Gamma)K_{II}^i\right) \\
& + Z_0(\xi,\eta,\rho)\left(h_u(\xi,\eta,\rho) - \sum_{j=1}^{m} N_j(\xi,\eta,\rho)h_{uj}\right)\left(\sum_{i=1}^{ntip} N_i(\Gamma)K_{III}^i\right)
\end{aligned}
\tag{1}
$$

In (1), ξ, η and ρ are the local enriched element coordinates and u_j are the nodal displacements. N_j are the regular finite element shape functions and Z_0 is a zeroing function which is 1 for all enriched elements. f_u, g_u and h_u are the analytically known terms from asymptotic crack tip displacement expressions for mode-I, -II and -III displacement components and m = 20 or 10 depends on element type. K_I^i, K_{II}^i and K_{III}^i are the unknown nodal SIFs at the i^{th} crack front node, and the serie $\left(\sum_{i=1}^{ntip} N_i(\Gamma)K_{I,II,III}^i\right)$ symbolizes SIF variations along the crack front on the element edge. *ntip* is 3 for a quadratic element and Γ is the local isoparametric coordinate varies between −1 and 1. As can be seen from the above formulation, the SIFs are directly embedded in the formulation of enriched elements and thus, they are computed automatically using FRAC3D without any post-processing.

The crack growth model introduced by Paris-Erdogan (Paris and Erdogan, 1963) and modified by Tanaka (Tanaka, 1974) for mixed mode

Table 1
Coefficients of ΔK_{eq} (Eq. (4)).

a	b	c	d	e
0.5263	0.3322	−0.1112	0.0257	−0.0004

Table 2
Coefficients of crack deflection angle (θ_0) equation (Eq. (5)).

a	b	c	d
0.1723	5.1062	−2.7483	−1.1636

problems is used to predict fatigue crack growth rate;

$$\frac{da}{dN} = C\left(\Delta K_{eq}\right)^n \tag{2}$$

In (2), N is the number of loading cycles, a is the crack length, C and n are the material constants and ΔK_{eq} is the equivalent SIF range, which describes the combination of basic modes under mixed mode conditions.

In previous studies (Ayhan and Demir, 2019; Demir et al., 2019; Yaren et al., 2019), mixed mode-I/III and I/II/III fracture tests were carried out for compact tension-shearing and tearing (CTST) specimen under different mode mixity loading conditions. The test results showed high level of inconsistencies on prediction of unstable fracture load magnitudes between three-dimensional fracture criteria existing in the literature and experimental results for dominant mode-II and -III loading cases. Hence, improved equivalent SIF equations had been developed using critical fracture loads obtained from the tests and K_I, K_{II}, and K_{III} SIFs computed from numerical fracture analyses. Those developed equations (Eqs. 3 and 4) from the corresponding studies (Ayhan and Demir, 2019; Demir et al., 2019; Yaren et al., 2019) are used to predict ΔK_{eq}, of which Eq. (3) defines the relation between the coupled mode-II and -III SIFs. By combining Eq. (3) with mode-I cyclic SIF, Eq. (4) expresses ΔK_{eq} for mixed mode-I/II/III fatigue crack growth problems;

$$\Delta K_{eq(II-III)} = \sqrt{0.6890\Delta K_{II}^2 + 0.6796\Delta K_{III}^2} \tag{3}$$

$$\Delta K_{eq} = \sqrt{a\Delta K_I^2 + b\Delta K_{eq(II-III)}^2 + c\Delta K_I \Delta K_{eq(II-III)}} + \left(d\Delta K_I^4 + e\Delta K_I \Delta K_{eq(II-III)}^3\right)^{0.25} \tag{4}$$

The coefficients of Eq. (4) are given in Table 1. As mentioned in the Introduction section, since crack deflects from its plane under mixed mode loading, to predict the incremental following crack profile, the crack deflection angles (θ_0) for all nodes along the crack front need to be determined.

In another previous study (Demir et al., 2017), mixed mode-I/II fracture tests were carried out for two different specimen types (compact tension shear-CTS and T-specimen) under different mixed mode loading conditions and using the obtained crack deflection angles from the experimental fracture tests and numerical fracture analyses, an improved equation had also been developed. The criterion (Eq. (5)) developed by Demir et al. (Demir et al., 2017) is used to provide crack deflection angle (θ_0) at a given crack front node based on its mixed mode SIFs;

$$\theta_0 = -arccos\left(\frac{aK_{II}^2 + K_I\sqrt{K_I^2 + bK_{II}K_I} + cK_{II}K_I}{K_I^2 + dK_{II}^2}\right) \tag{5}$$

Table 2 summarizes the coefficients of Eq. (5). The incrementally and nonplanarly growing crack surfaces are generated by predicting and successively adding the following crack front profiles to previous crack surfaces. This process is repeated in a loop setup as described in Fig. 2 until K_{eq} exceeds fracture toughness (K_{Ic}) of the material analyzed in the study. Non-planar crack growth modeling process involves many challenging tasks. In consequence of the lack of automatic fitting and re-meshing capability for non-planar crack surfaces, the procedure needs some manual intervention.

3. Numerical analyses

In this section, results of numerical analyses carried out by FCPAS for 3-D non-planar crack growth are presented. First, a circular rod with an

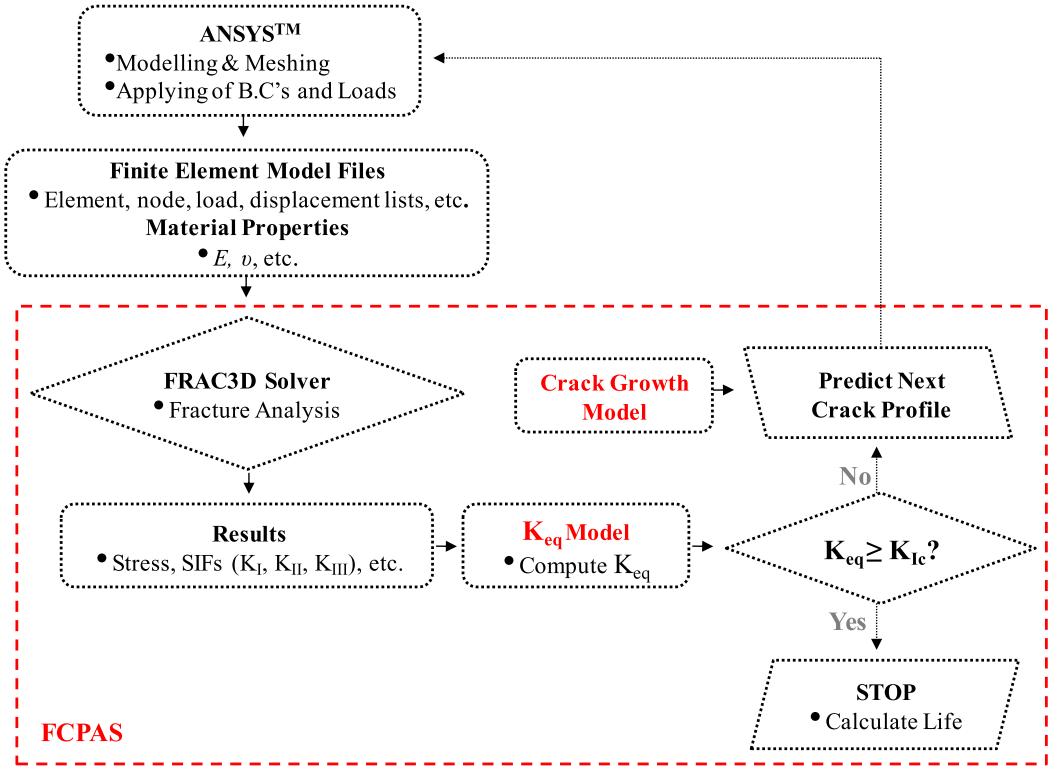

Fig. 2. Simulation process for three-dimensional non-planar crack growth (Ayhan, 2011).

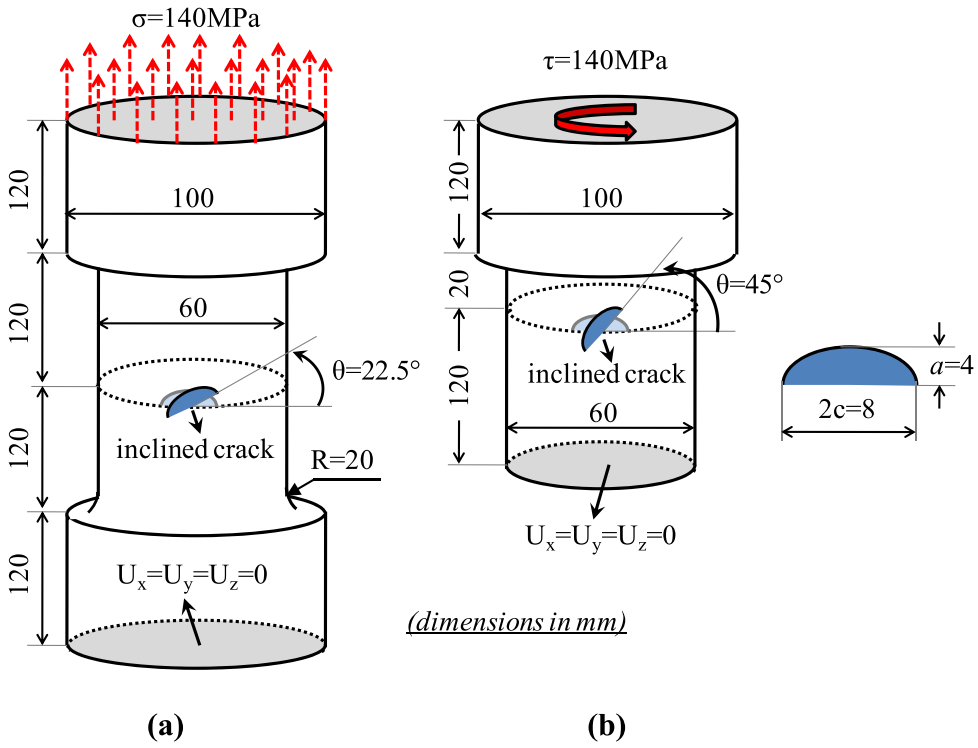

Fig. 3. Details of the problems subjected to fatigue loads, **(a)** tension, **(b)** torsion.

inclined initial crack subject to tension fatigue and torsion loads is considered. As a second numerical example, a hollow shaft containing an initial semi-elliptical crack under bending fatigue load is analyzed. Finally, analysis results of an H-shaped specimen with a semi-circular crack subject to tension fatigue load are summarized.

3.1. A cylindrical bar with an inclined initial crack

Non-planar fatigue crack growth analyses on a round bar specimen containing an inclined crack are carried out for two different loading conditions: pure tension and pure torsion. These cases were analyzed numerically in (Okada et al., 2013) using virtual crack closure-integral method (VCCM) to compute the SIFs and the criteria by Richard et al. (Richard et al., 2003) were used to predict the ΔK_{eq} and the crack deflection angle (θ_0). In Fig. 3, the geometric and loading details of the problem are summarized. The initial crack dimensions given in the figure are the same for both loading cases considered. A uniform tensile stress, $\sigma = 140$ MPa and a uniform torsional stress, $\tau = 140$ MPa

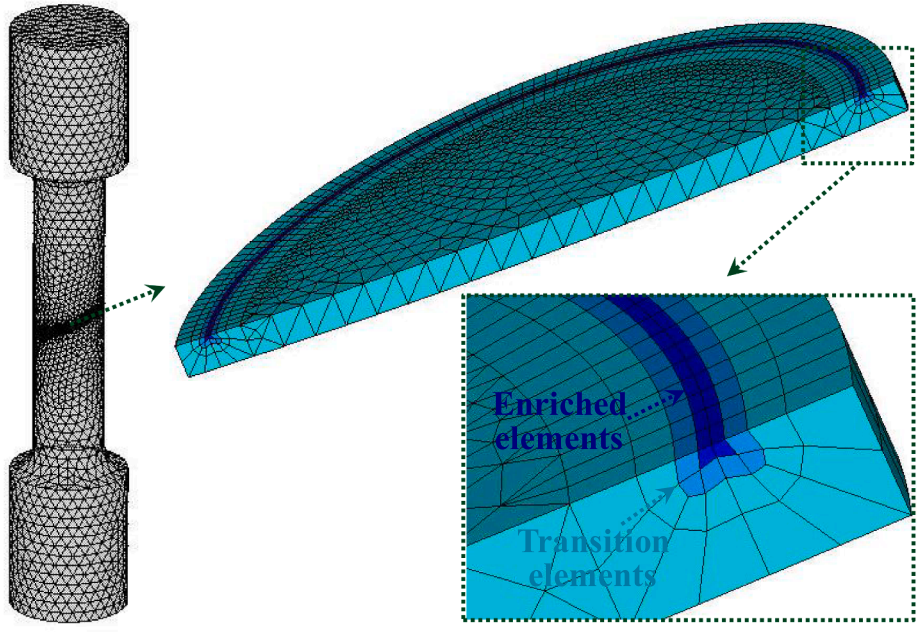

Fig. 4. General view of the overall model and zoomed view of crack region containing hexahedral enriched and transition elements.

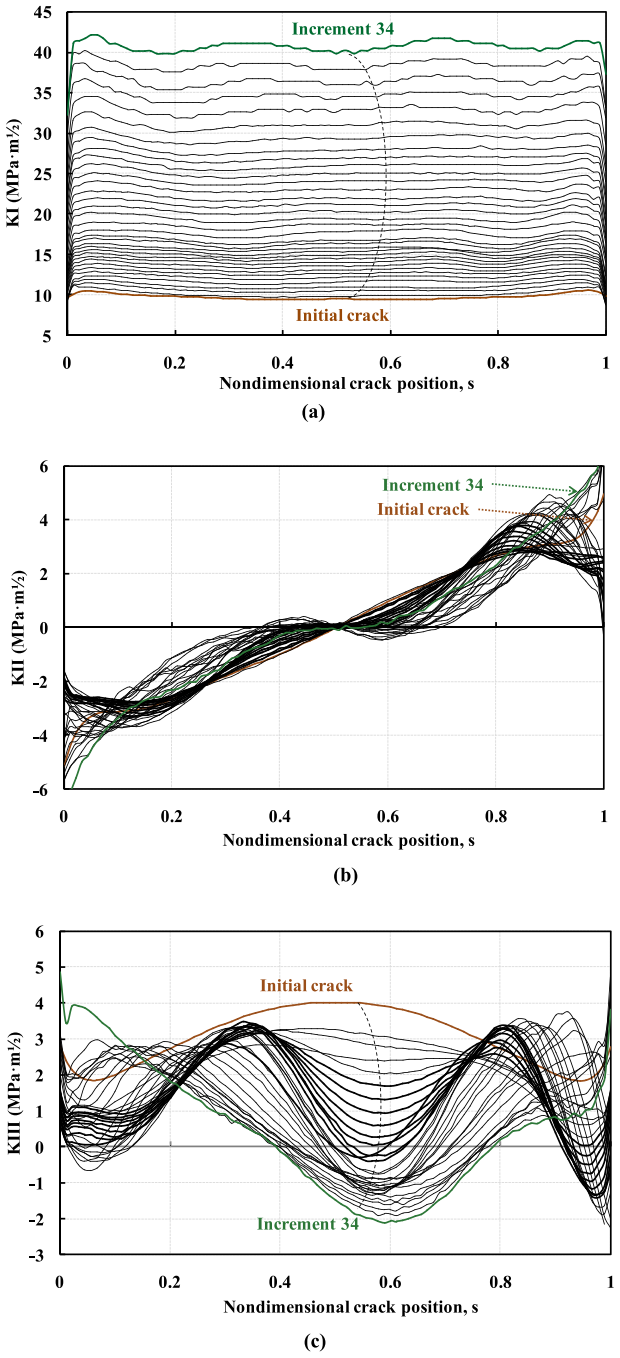

Fig. 5. SIFs along the crack front for all crack propagation steps performed for tension fatigue loading, **(a)** K_I, **(b)** K_{II}, **(c)** K_{III} distribution.

are applied to the cracked rod for the first and second loading cases, respectively. Fatigue crack growth analyses are performed at a stress ratio of R = 0 for both cases. The material considered for this application is a stainless steel. The material constants, C and n used for the analyses are 2.05×10^{-9} (mm/cycle·(MPa $\times$ $m^{0.5}$)) and 3.3, respectively. The fracture toughness value (K_{Ic}) is assumed to be 72 MPa $\times$ $m^{0.5}$. Overall view of the cracked finite element model and zoomed view of the crack region containing hexahedral enriched and transition elements along and near the crack front are shown in Fig. 4. As shown in the figure that enriched elements surround the crack front and transition elements are located between enriched elements and regular finite elements. In Fig. 5, SIF distributions along the crack front for all crack propagation steps performed for tension fatigue loading are given. The crack growth analyses are finalized after the 34th incremental step of the propagation. It is seen from Fig. 5 that, as expected, K_I increases with crack growth. K_{II} SIF changes from negative to positive anti-symmetrically along the crack front and the distributions are almost similar for all propagation steps. In Fig. 6, overall view of the finite element model for the last propagation step and zoomed view of the mesh around the crack front are given by changing the level of translucency of the rest of the crack surface elements to see the crack growth trajectory within the whole model. The finite element models are meshed using hexahedral enriched elements in a tube-like domain along the crack front and the remaining model is discretized using tetrahedral finite elements for each analysis step. The model shown in Fig. 6 has 256,482 nodes and 157,986 tetrahedral elements (10-noded). It can be checked with the reference study (Okada et al., 2013) that closely resembling propagating crack front profiles, which were the only available data for this case, are obtained in the current study. The predicted number of cycles vs. crack depth curve for the case of tension fatigue loading is shown in Fig. 7.

As in the first application case (tension loading), non-planar fatigue crack propagation analyses are also carried out for the second case in which the specimen is subjected to torsion fatigue loading. The close-up view of the finite element model around the crack region for the initial crack and comparison of the resulting SIFs along the crack front computed in the current study and in the study of Okada et al. (Okada et al., 2013) are given in Figs. 8 and 9. 172,870 tetrahedral elements and 246,209 nodes are included in the presented finite element model (Fig. 8). It is seen from Fig. 9 that SIF distributions along the initial crack front are almost identical with the data of the reference study. Crack propagation analyses are terminated after 32 steps of increment. Variations of SIFs along the entire crack front for each increments under torsion loading are plotted in Fig. 10. It is observed with crack growth that, K_I increases on one of the free-surface much more than the other free surface. Therefore, as the crack grows, further crack growths would be expected for the free-surface point for which higher K_I SIFs are observed. K_{II} and K_{III} SIFs increase slightly with crack growth. Non-planar crack propagation analysis process is terminated for torsion loading case after the 32nd step. Zoomed views of crack region with different perspectives for the last step of the analyses and comparison of predicted crack paths with the numerical and experimental crack growth data of the study (Okada et al., 2013) are shown in Figs. 11 and 12, respectively. The three-dimensional twisted crack paths are projected on the initial crack plane for which reference axis is presented in Fig. 11. The x-y plane corresponds to the initial crack plane and z-axis is perpendicular to its plane. In the reference study (Okada et al., 2013), experimental crack growth surface marked for few crack profiles to compare with their numerical propagation predictions was presented. In order to compare the crack propagation profiles with the reference study, the predicted crack paths close in size to the given paths were plotted. As indicated above, it can be clearly seen from both of the figures that one of the free surface grows much further compared to the another one. Fig. 12 shows that the crack growth predictions made by FCPAS and the reference study are very close to each other and the profiles measured from the experiments propagate at the depth point more than the numerical predictions.

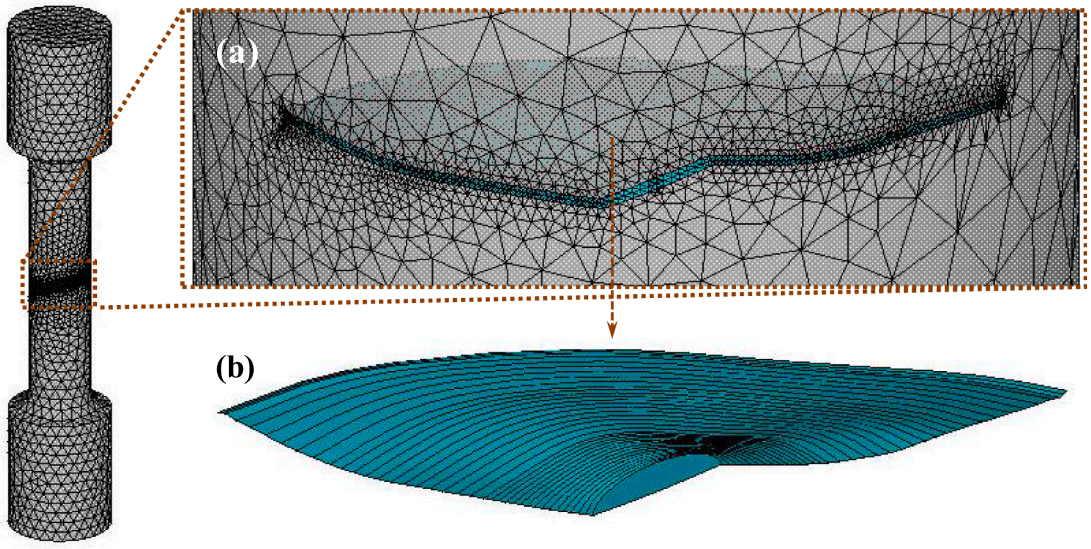

Fig. 6. Finite element model for the last propagation step, **(a)** zoomed view of the mesh around the crack front, **(b)** crack growth path.

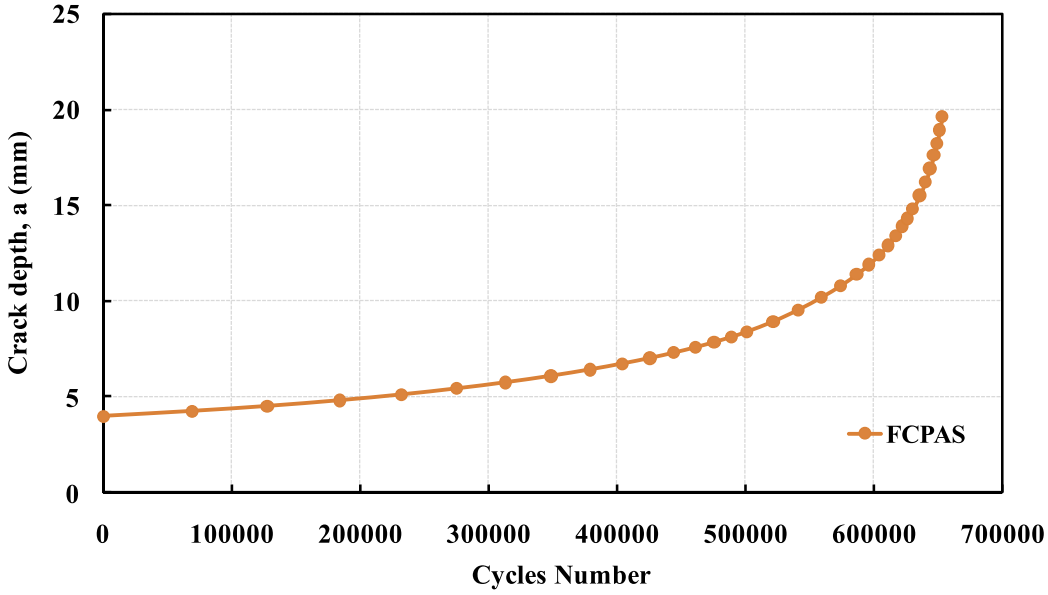

Fig. 7. Predicted crack depth length as a function of number of cycles.

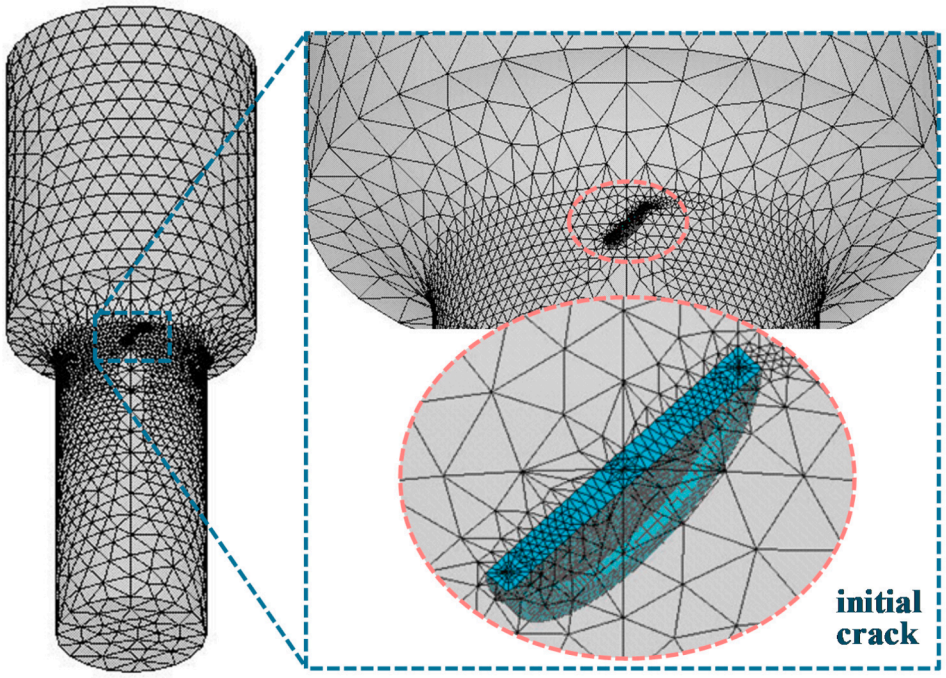

Fig. 8. General view of the overall model and close-up view of finite elements around the initial crack region under torsion loading case.

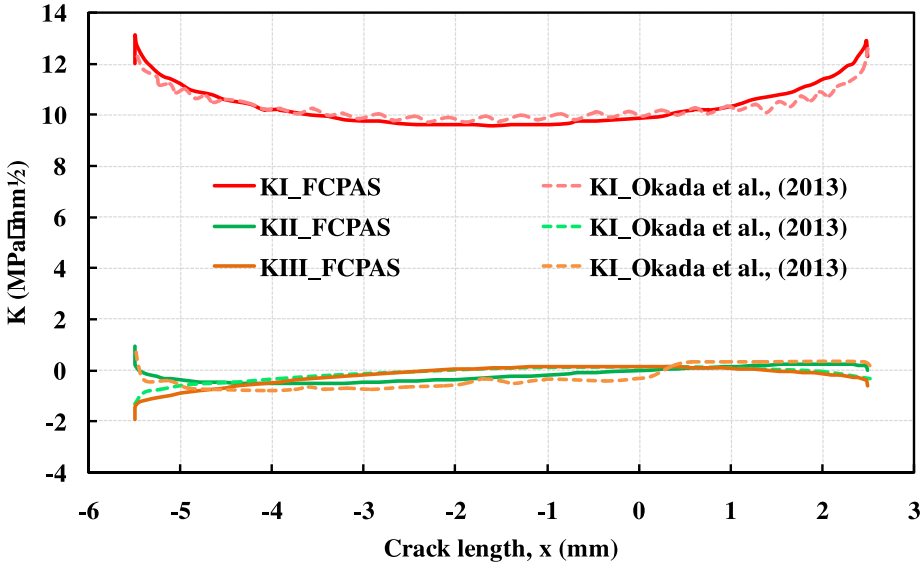

Fig. 9. Comparison of the computed SIFs along the crack front with the study of Okada et al. (2013).

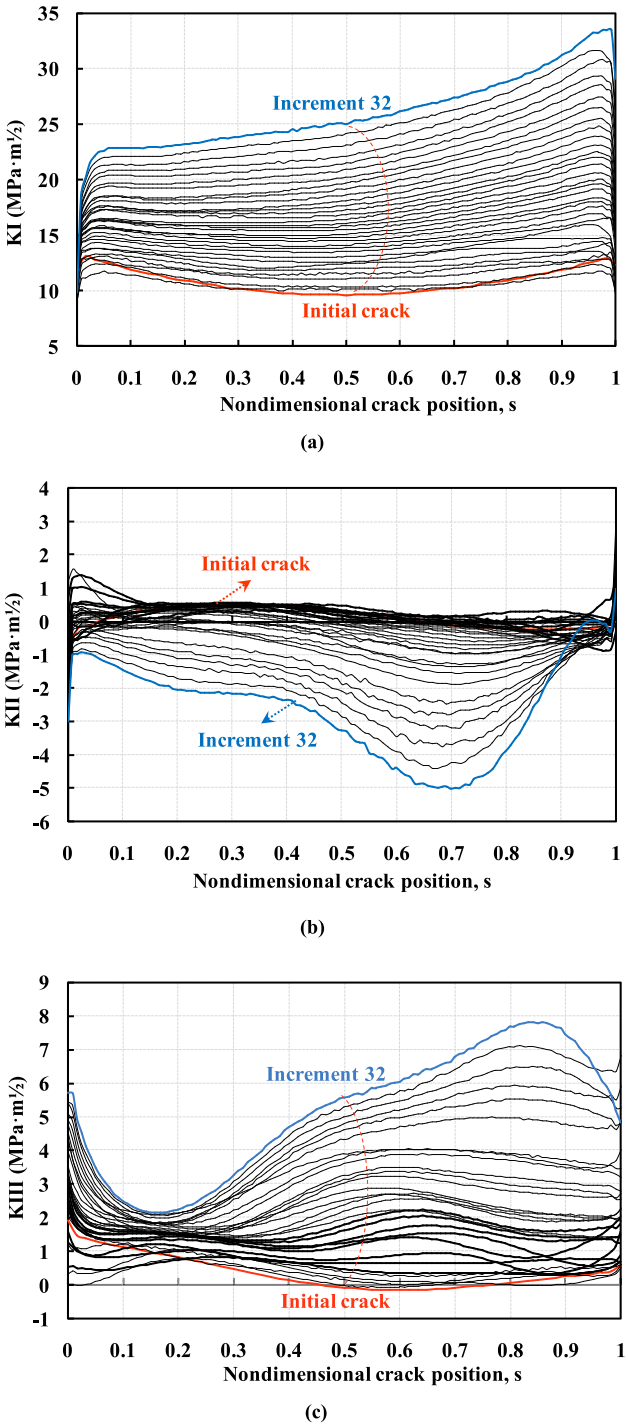

Fig. 10. Distributions of SIFs along the crack front for each crack propagation steps performed for torsion fatigue loading, **(a)** K_{I}, **(b)** K_{II}, **(c)** K_{III} variation.

The possible cause may be related to the crack tip plasticity. The probable presence of local plasticity on crack tip free surfaces may retard crack propagation. In Fig. 13, a comparison of fatigue crack propagation lives predicted for the specimen subjected to torsional load is plotted as a

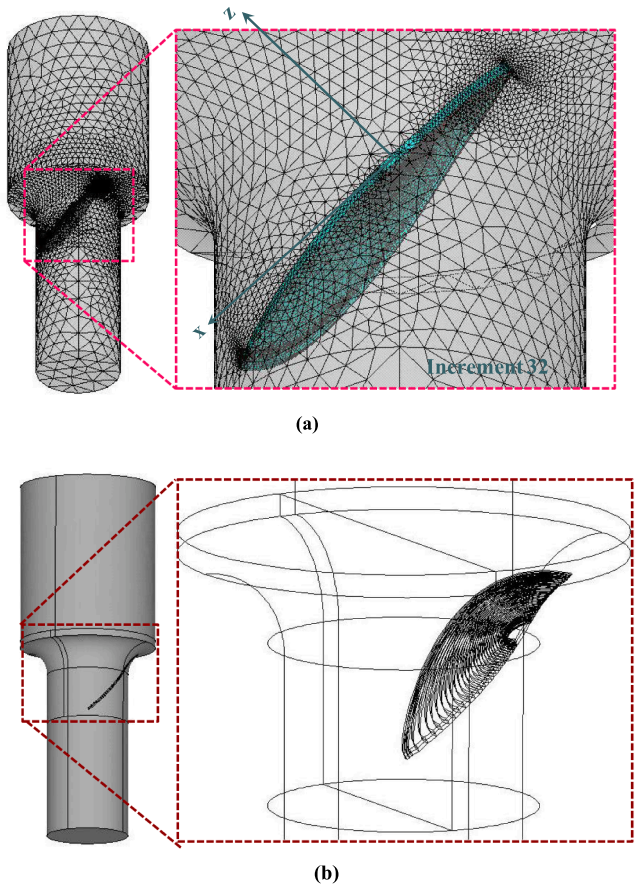

Fig. 11. Zoomed perspective views of crack region for the 32nd propagation step under torsion loading case, (a) finite element model, (b) incremental crack profiles.

function of surface crack length. The curve lengths of the incrementally growing edge-point on the crack front are measured and cumulatively added up to calculate the value of free surface crack length during the simulation procedure. Experimental test was carried out at the stress ratio (R) of −0.9 in the reference study (Okada et al., 2013). For the case of R = −0.9, one needs to first realize that two sides of the loading cycle, i.e., positive and negative torsional loading, in fact yield opposite crack driving forces, i.e., if the crack surfaces open when positive torque is applied, they would be closed during the negative portion of the torque cycle. This is because the crack plane which makes a 45° angle with the axis of the cylindrical specimen will be subjected to tensile normal stress in one half of the cycle, while it will experience negative normal stress during the other half. Therefore, since the compressive normal stress acting on the crack plane will not contribute to crack growth due to closure of crack surfaces under compressive remote loading, it is anticipated that the fatigue crack propagation behavior of the case with R = −0.9 would be close to that of R = 0, and thus is not included as a separate curve in Fig. 13. It should be stated that FCPAS gives closer predictions to the experimental life and remarkable difference exist between the numerical predictions.

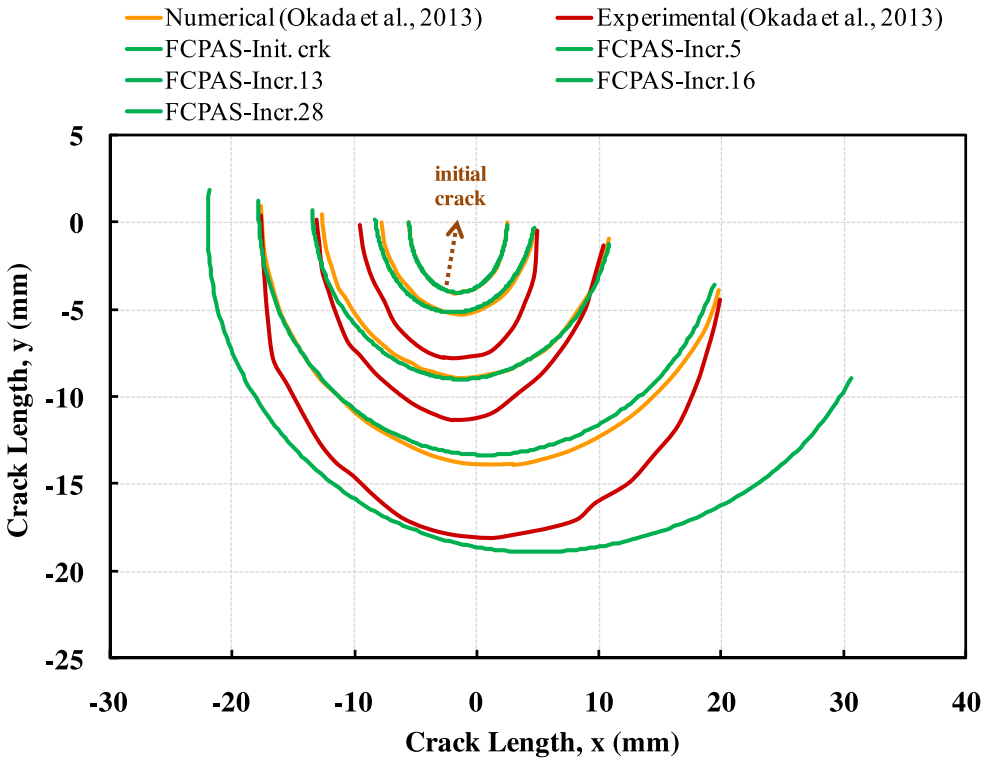

Fig. 12. Comparisons of predicted crack profiles with the numerical and experimental crack growth data of the study (Okada et al., 2013).

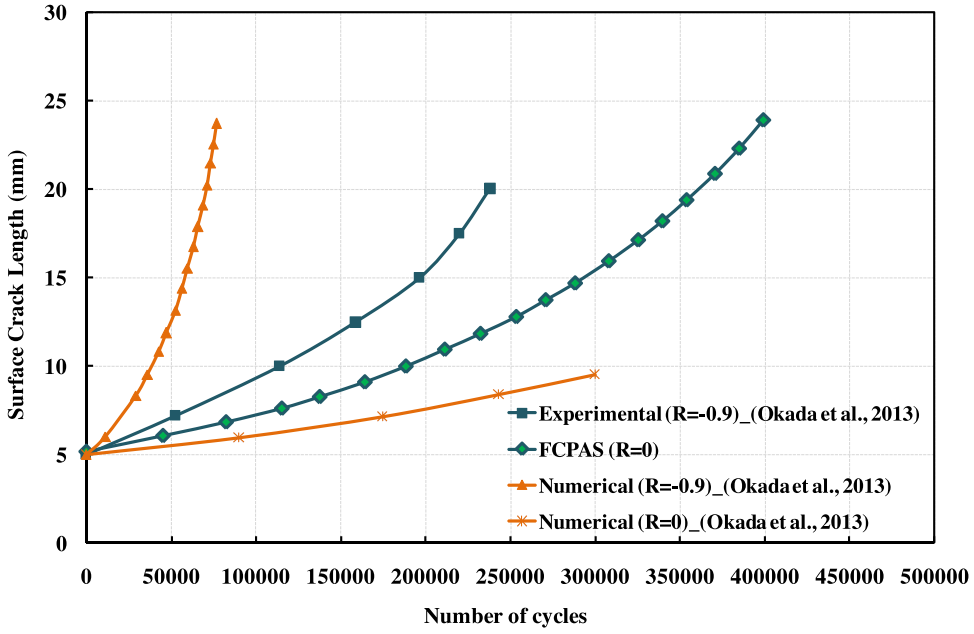

Fig. 13. Comparisons of predicted crack propagation lives for the case subjected to torsion load.

3.2. A hollow shaft with a semi-elliptical surface crack

The study by Citarella et al. (2018) is considered as the second application problem. In Fig. 14, detailed dimensions and finite element model of hollow shaft with a zoomed view of initial crack zone are given. As seen from the figure, the shaft containing the semi-elliptical crack is subject to bending load. The symmetry boundary condition is implemented on the surface nodes of the boundary which is defined as symmetry plane in the figure. 200 kN bending load (R = 0) is applied uniformly in the opposite (y-axis) direction on nodes located in both force plane. Numerical simulations were performed using three different codes by Citarella et al. (2018) and similar results were obtained in terms of prediction of SIFs and crack growth surfaces. Simulation results in the current study are compared with the data (Citarella et al., 2018) obtained using the code, BEASY, in which the boundary element method and Tanaka criterion (Tanaka, 1974) given in Eq. (6) were used to compute the SIFs and ΔK_{eq}, respectively.

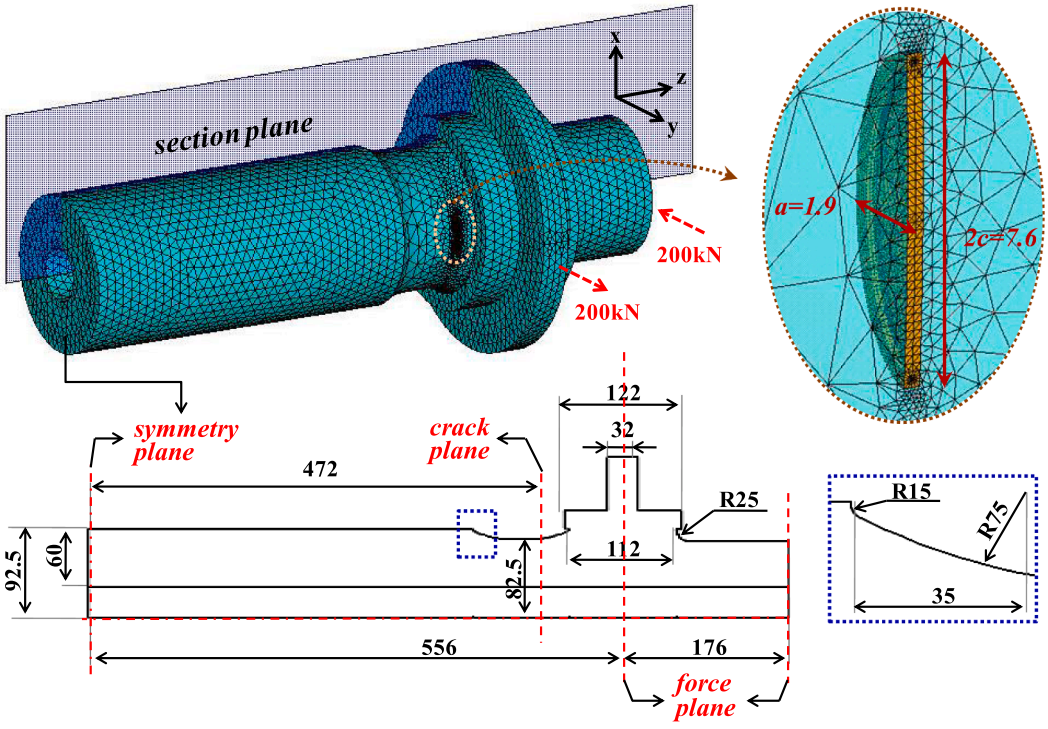

Fig. 14. Detailed dimensions of hollow shaft with a zoomed view of the finite element model containing the initial crack.

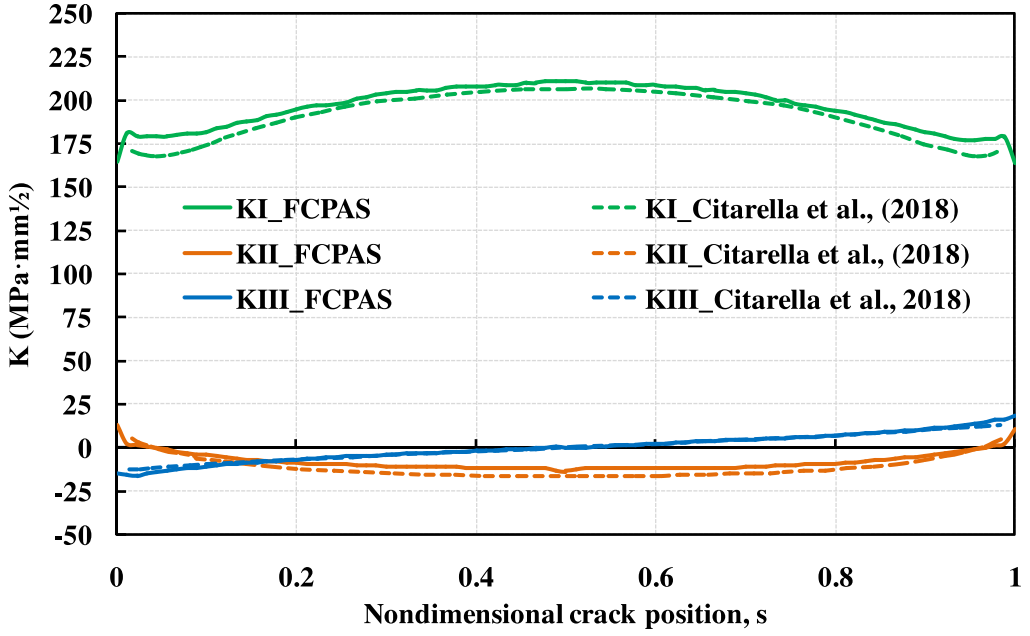

Fig. 15. Distributions of mixed mode SIFs along the initial crack front.

$$\Delta K_{eq} = \left[\Delta K_I^4 + 8\Delta K_{II}^4 + \frac{8\Delta K_{III}^4}{1-\nu}\right]^{0.25} \quad (6)$$

In (6), ν is Poisson's ratio. The crack growth related material constants for the material made of steel alloy, C and n are 1.23085×10^{-12} (mm/cycle·(MPa $\times$ mm$^{0.5}$)) and 2.8, respectively. The value of (K_{Ic}) is assumed to be 100 MPa $\times$ m$^{0.5}$. Fig. 15 shows the comparison of SIF distributions for the initial crack obtained from the current study using FCPAS and from the reference study (Citarella et al., 2018) using BEASY. Trends in variation of mixed mode SIFs agree well with each other.

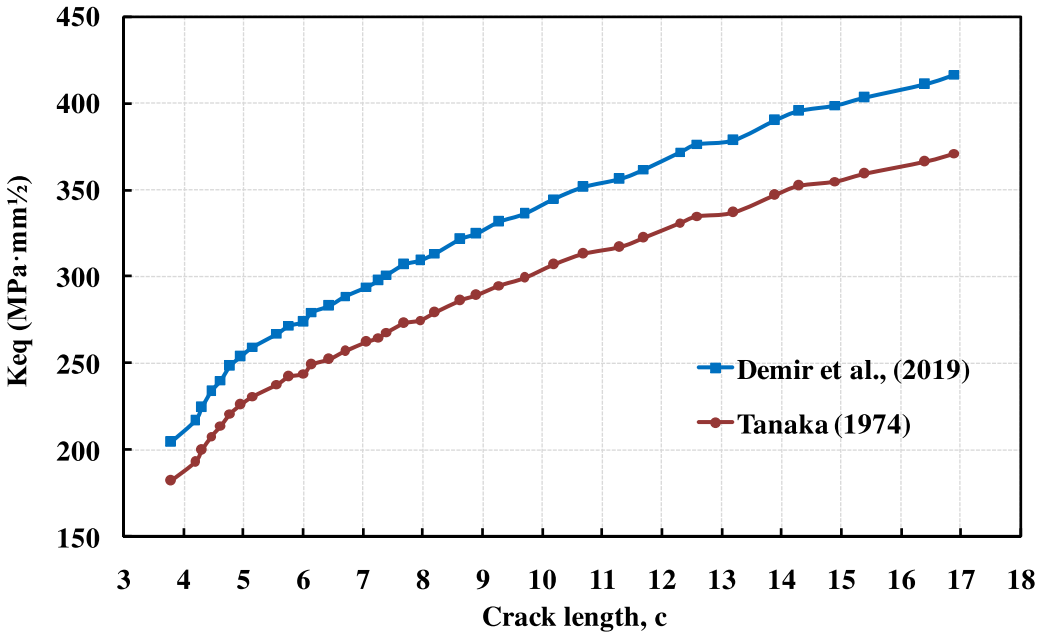

Fig. 16. Variation of the resulting K_{eq} vs. edge crack length during crack growth.

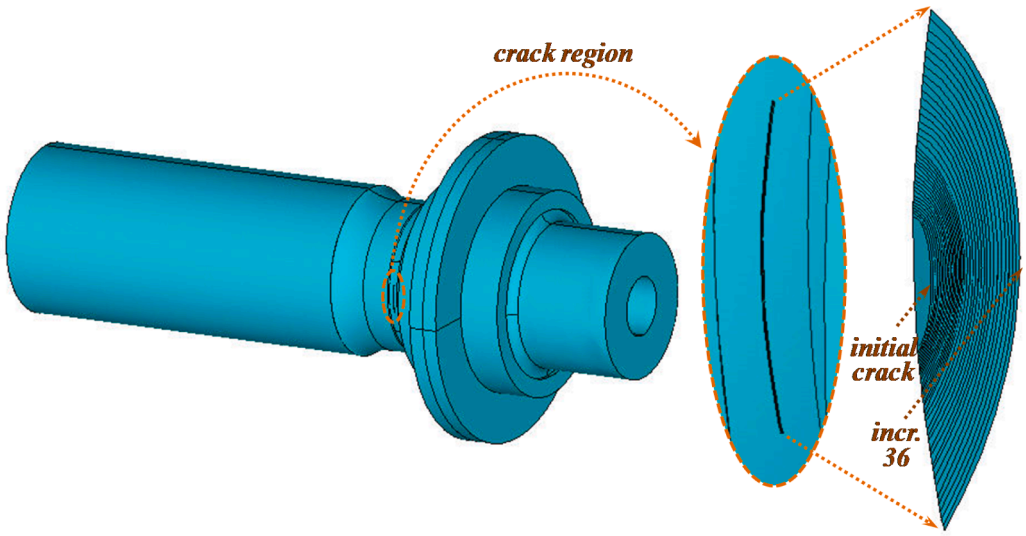

Fig. 17. Close-up view of the cracked region and evolving crack surfaces.

The K_{eq} SIFs according to the criterion (Eqs. 3 and 4) proposed by Demir et al. (2019) and the criterion (Eq. (6)) proposed by Tanaka (1974) are computed using the resulting SIFs obtained by FCPAS for the crack front edge points of all evolving crack fronts. Variation of the computed K_{eq} SIFs as a function of edge crack length is given in Fig. 16. It is seen that as crack grows overall tendencies for both criteria are similar and the predictions by Demir et al. (2019) are relatively higher. The successive non-planar crack growth analyses are terminated after 36 steps of crack increments. Overall and close-up views of the cracked region and comparison of predicted crack growth lives from the current and the reference study (Citarella et al., 2018) are shown in Figs. 17 and 18, respectively. From Fig. 18, the lives predicted with respect to the Demir et al. (2019) and the Tanaka (1974) criteria in the current study using the resulting SIFs from FCPAS are seen to agree well with the predictions of the reference study (Citarella et al., 2018).

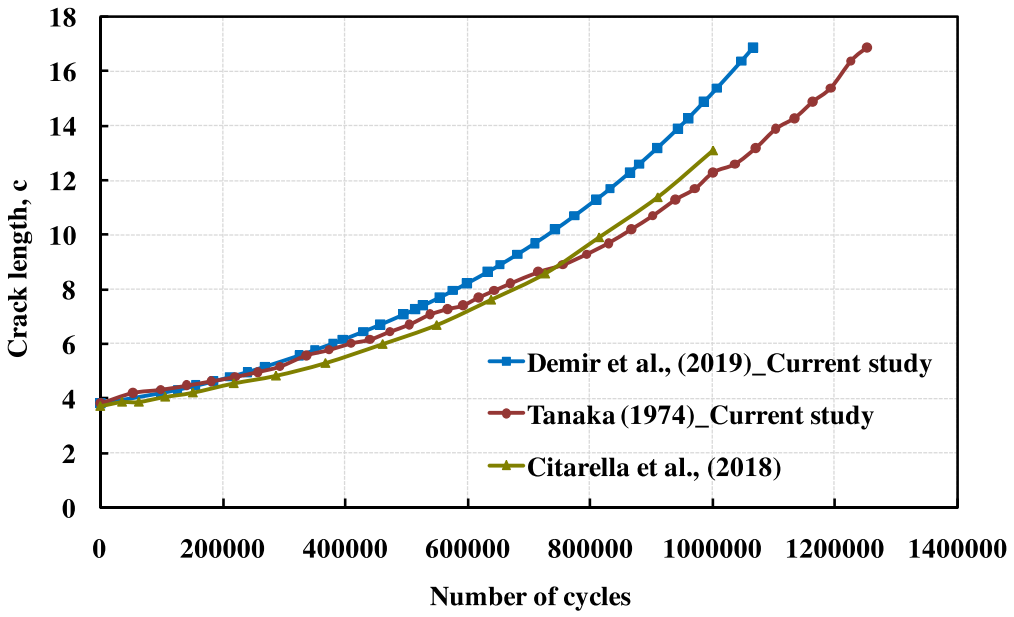

Fig. 18. Comparison of the predicted crack growth lives with reference to the current and the reference study (Citarella et al., 2018).

3.3. *H-shaped specimen with an initially deflected semi-circular crack*

The study by Grasso et al. (Grasso et al., 2018) is considered as a final application case. Non-planar crack growth analyses are performed for the specimen having a cross section similar to H-shape and containing an initially deflected semi-circular surface crack. Fig. 19 presents the details of the geometry and its dimensions. It is seen that the initial surface crack is deflected with the angle of 45° and the specimen is subjected to

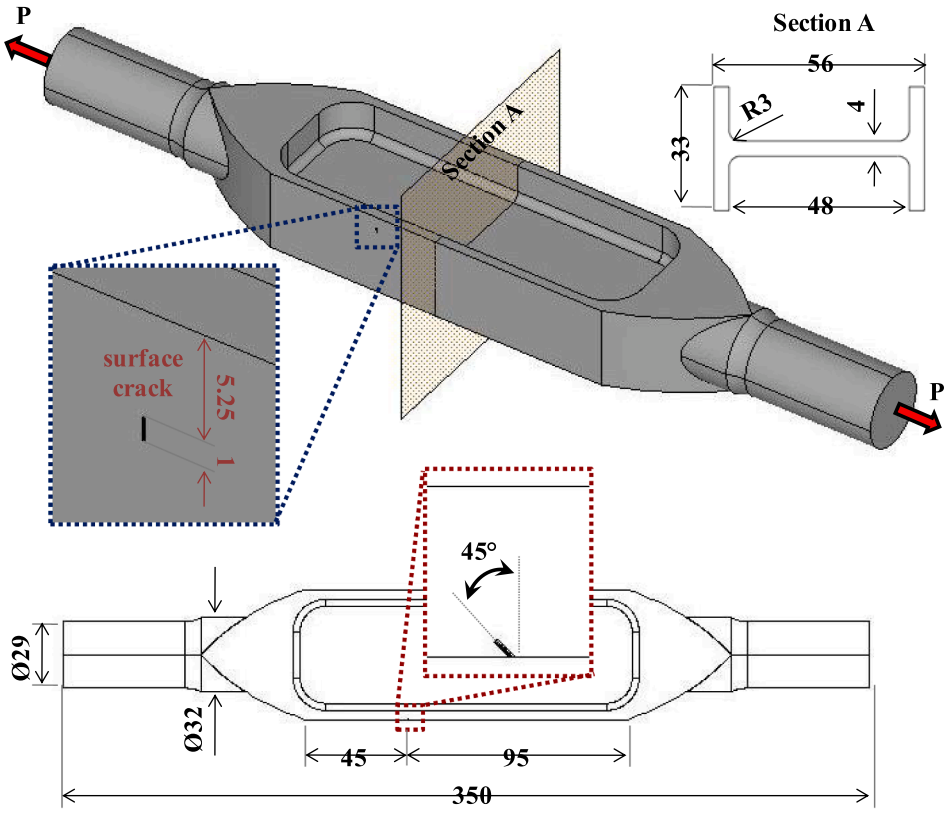

Fig. 19. Details of the H-shaped specimen geometry and its dimensions.

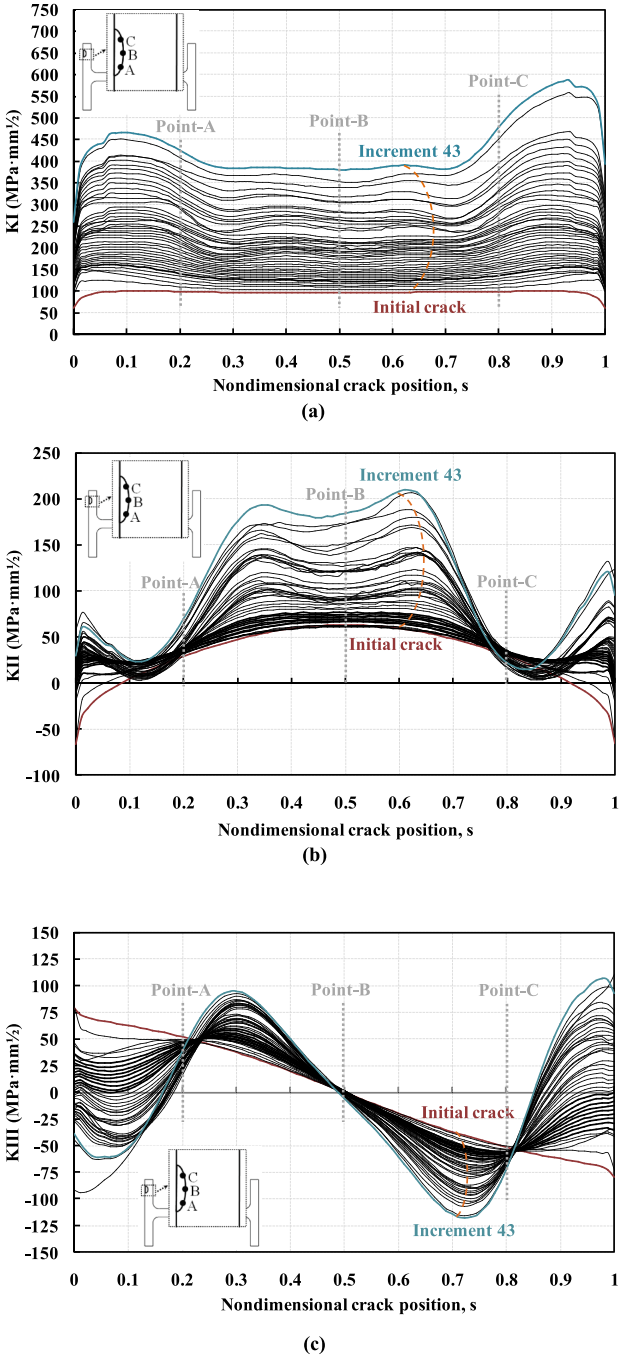

Fig. 20. Mixed mode SIF distributions along the crack front for each incremental crack propagation step, **(a)** K_{I}, **(b)** K_{II}, **(c)** K_{III} variation.

tension load, which causes mixed mode fracture conditions around the crack region.

The material used is aluminum alloy F357. The applied pressure at the specimen ends is 126.37 MPa, which generates 180 MPa of normal stress at the cross-section containing the initial crack. The initial surface crack has a total surface length of 1 mm and a depth of 0.5 mm. The equations (7, 8 and 9) were used to compute the ΔK_{eq} and the NASGRO equation (10) was employed as crack growth model and the criterion by Erdoğan and Sih (Erdogan and Sih, 1963) was used to predict crack deflection angle in the reference study (Grasso et al., 2018).

$$\Delta K_{eq} = K_{eq,max} - K_{eq,min} \tag{7}$$

$$K_{eq,max} = \sqrt{K_{I,max}^2 + \left(\beta_{II} K_{II,max}\right)^2 + \left(\beta_{III} K_{III,max}\right)^2} \tag{8}$$

$$K_{eq,min} = \sqrt{K_{I,min}^2 + \left(\beta_{II} K_{II,min}\right)^2 + \left(\beta_{III} K_{III,min}\right)^2} \tag{9}$$

$$\frac{da}{dN} = C\left(\left(\frac{1-f}{1-R}\right)\Delta K\right)^n \frac{\left(1 - \frac{\Delta K_{th}}{\Delta K}\right)^p}{\left(1 - \frac{K_{max}}{K_C}\right)^q} \tag{10}$$

where, $\beta_{II} = K_{IIC}/K_{IC}$, $\beta_{III} = K_{IIIC}/K_{IC}$, N is the number of loading cycles, a is the crack length, C, n, p, q are the empirical constants, R is the stress-ratio, K_{max}, K_{min} are the SIFs of the maximum and minimum loading forces in the cycle, ΔK is the SIF range, ΔK_{th} is the threshold of SIF, K_c is the critical value of SIF referred to fracture toughness and f is the Newman's crack opening function.

The fatigue crack growth-related material constants, C and n, are 3.0447×10^{-11} (mm/cycle·(MPa $\times$ $\mathrm{mm}^{0.5}$)) and 2.54, respectively. The load ratio is $R = 0.1$. The value of (K_{Ic}) is assumed to be 33 MPa $\times$ $\mathrm{m}^{0.5}$. Fig. 20 shows the mixed mode SIF distributions along the crack front for the carried out 43 steps of crack propagation analyses. It is seen from Fig. 20a that during crack growth, mode-I SIFs increase towards the vicinity of the crack surface compared to the crack front center and include sudden drops towards the close vicinity of the free-surface. K_{II} SIFs increase around the crack front center much more than the vicinity of the crack edges and remarkable drops and jumps are observed towards the crack edges. As crack grows, K_{III} SIFs vary anti-symmetrically with regard to the center point of the crack along the crack front (Fig. 20c). In Fig. 21, comparisons of computed K_{I} SIFs as a function of relative cumulative crack length are plotted for three points on the crack front. It is seen from the FCPAS solutions that much further relative cumulative crack lengths are obtained for the free surface points as compared to the center point of the crack front. As crack grows, variation of K_{I} SIFs for the free surfaces are almost identical for each increment. Close-up view of finite element mesh around the crack region and crack growth trajectories for the last propagation step for which 175,295 tetrahedral elements and 311,356 nodes are used are given in Fig. 22.

Finally, in Fig. 23, comparison of fatigue life predictions are presented as a function of crack length. In order to show the importance of the ΔK_{eq} and the crack growth models used for crack propagation analysis, the computed SIFs (Fig. 20) using FCPAS are employed to compute the ΔK_{eq} (Eqs. 7, 8 and 9), from which the fatigue life (Eq. (10)) is predicted. The computed life curve, labeled as FCPAS_(NASGRO Eq), is presented in Fig. 23. It is worthwhile to note from Fig. 21 that for a given relative cumulative crack length, K_{I} SIFs computed by FCPAS are smaller than the reference study (Grasso et al., 2018). Thus, as expected, greater fatigue life is obtained by FCPAS when using the same crack growth model of Ref. (Grasso et al., 2018) (Fig. 23).

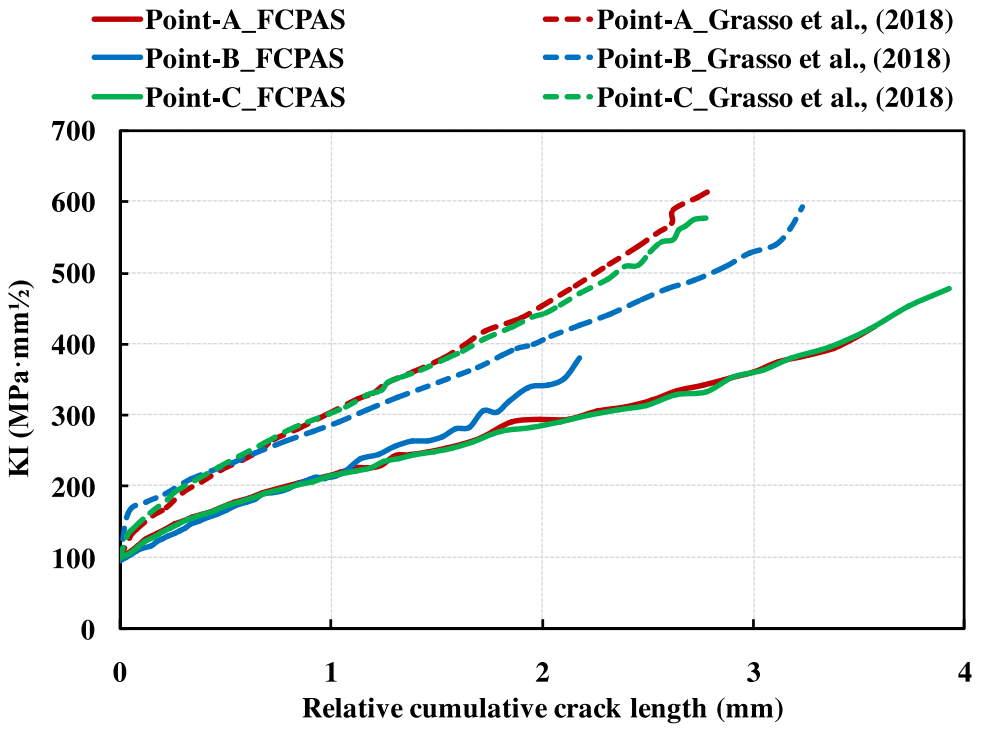

Fig. 21. Variation of the computed K_I SIFs vs. relative cumulative crack length during crack growth.

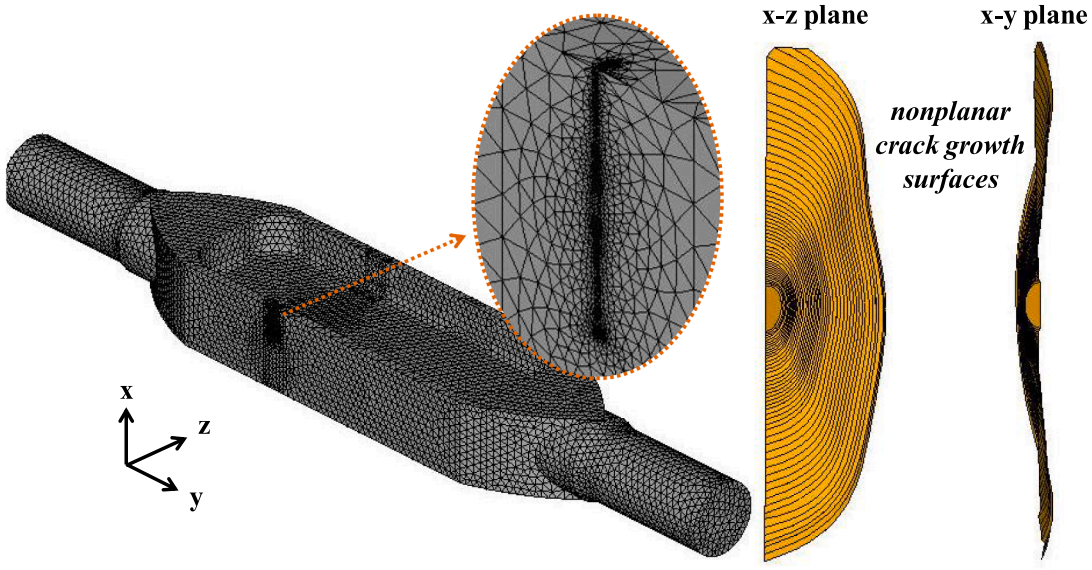

Fig. 22. Close-up view of finite element mesh around the cracked region and crack growth trajectories for the last propagation step.

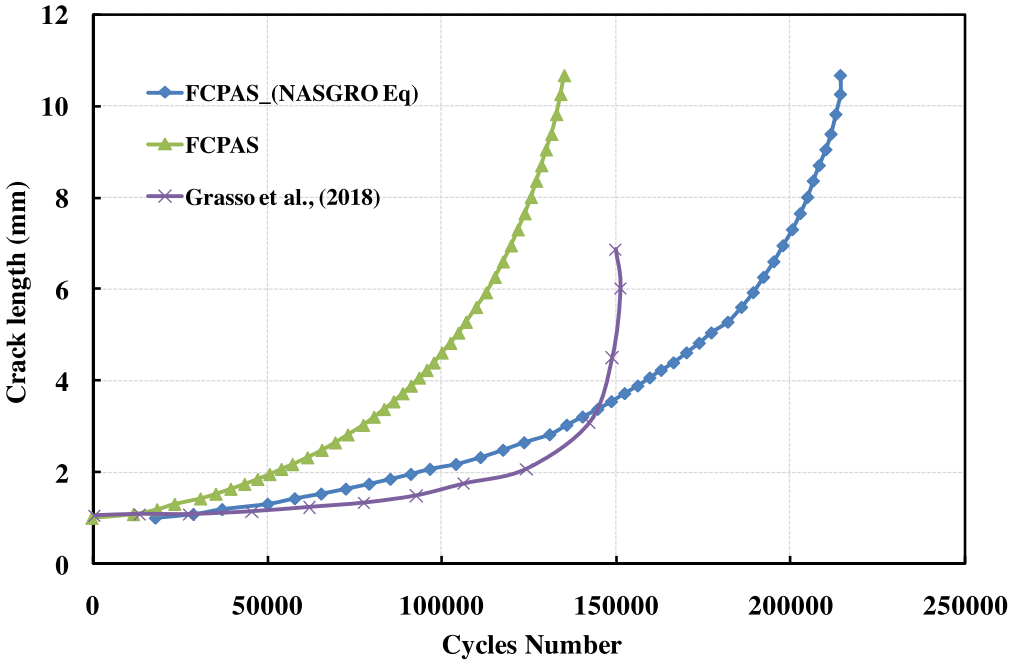

Fig. 23. Crack lengths as a function of predicted number of cycles.

4. Summary and conclusions

In this study, mixed mode non-planar fatigue crack propagation simulations are performed for different case studies selected from the literature. The crack growth analyses are carried out using Fracture and Crack Propagation Analysis System (FCPAS), which employs enriched finite elements surrounding crack front to calculate the mixed mode SIFs. The recently developed fatigue crack growth criterion by the authors is used to predict the K_{eq} SIF and crack deflection angle. The results from numerical analyses show that good agreements are obtained between the data from the literature in terms of computation of SIFs, prediction of evolving crack trajectories and fatigue crack growth lives. Thus, it is concluded that FCPAS is capable to perform three-dimensional non-planar fatigue crack propagation analyses and the recently developed fatigue crack growth criteria can be used to predict the non-planar successive incremental crack growth trajectories.

Declaration of Competing Interest

The authors declare that they have no known competing financial interests or personal relationships that could have appeared to influence the work reported in this paper.

Acknowledgement

The financial support by The Scientific and Technological Research Council of Turkey (TUBITAK) under Project Number: 217M690 for this study is gratefully acknowledged.

References

ANSYS, "Theory manual version 12.0, Ansys Inc." Canonsburg, PA, USA, 2009.
Ayhan, A.O., 2004. Mixed mode stress intensity factors for deflected and inclined surface cracks in finite-thickness plates. Eng. Fract. Mech. 71 (7–8), 1059–1079.
Ayhan, A., 2007. Mixed mode stress intensity factors for deflected and inclined corner cracks in finite-thickness plates. Int. J. Fatigue 29 (2), 305–317.
Ayhan, A.O., 2007. Stress intensity factors for three-dimensional cracks in functionally graded materials using enriched finite elements. Int. J. Solids Struct. 44 (25–26), 8579–8599.
Ayhan, A.O., 2009. Three-dimensional mixed-mode stress intensity factors for cracks in functionally graded materials using enriched finite elements. Int. J. Solids Struct. 46 (3-4), 796–810.
Ayhan, A.O., 2011. Simulation of three-dimensional fatigue crack propagation using enriched finite elements. Comput. Struct. 89 (9-10), 801–812.
Ayhan, A.O., Demir, O., 2019. A novel test system for mixed mode-I/II/III fracture tests–Part 1: Modeling and numerical analyses. Eng. Fract. Mech. 218, 106597.
Ayhan, A.O., Nied, H.F., 1998. FRAC3D-Finite element based software for 3-D and generalized plane strain fracture analysis. Semicond. Res. Corp. Tech. Rep.
Ayhan, A.O., Nied, H.F., 2002. Stress intensity factors for three-dimensional surface cracks using enriched finite elements. Int. J. Numer. Methods Eng. 54 (6), 899–921.
Ayhan, A.O., Kaya, A.C., Nied, H.F., 2007. Analysis of three-dimensional interface cracks using enriched finite elements. Int. J. Fract. 142 (3-4), 255–276.
B. J. Carter, A. R. Ingraffea, and T. N. Bittencourt, "Topology-controlled modeling of linear and nonlinear 3D crack propagation in geo-materials," in *Fracture of Brittle Disordered Materials: Concrete, Rock and Ceramics*, First edit., G. Baker and B. L. Karihaloo, Eds. E&FN Spon Publishers Brisbane, Australia, pp. 301–318, 1995.
Carter, B.J., Wawrzynek, P.A., Ingraffea, A.R., 2000. Automated 3-D crack growth simulation. Int. J. Numer. Methods Eng. 47 (1-3), 229–253.
Citarella, R., Giannella, V., Vivo, E., Mazzeo, M., 2016. FEM-DBEM approach for crack propagation in a low pressure aeroengine turbine vane segment. Theor. Appl. Fract. Mech. 86, 143–152.
Citarella, R., Giannella, V., Lepore, M., Dhondt, G., 2018. Dual boundary element method and finite element method for mixed-mode crack propagation simulations in a cracked hollow shaft. Fatigue Fract. Eng. Mater. Struct. 41 (1), 84–98.
T. J. Curtin, R. A. Adey, J. M. W. Baynham, and P. Marais, "Fatigue Crack Growth Simulation for Complex Three-Dimensional Geometry and Loading," in *NASA Conference Publication*, pp. 657–666, 1999.
Demir, O., Ayhan, A.O., 2018. Comparison of 3-D mixed mode fatigue crack growth analysis using different element types along the crack front. Proc. Book Fourth Internat. Conf. Adv. Mech. Eng.: ICAME 2018, 1609–1617.
Demir, O., Ayhan, A.O., İriç, S., 2017. A new specimen for mixed mode-I/II fracture tests: Modeling, experiments and criteria development. Eng. Fract. Mech. 178, 457–476.
Demir, O., Ayhan, A.O., İriç, S., 2019. A novel test system for mixed mode-I/II/III fracture tests – Part 2: Experiments and criterion development. Eng. Fract. Mech. 220, 106671.
Erdogan, F., Sih, G.C., 1963. On the crack extension in plates under plane loading and transverse shear. J. Basic Eng. 85 (4), 519–525.
Giannella, V., Perrella, M., Citarella, R., 2017. Efficient FEM-DBEM coupled approach for crack propagation simulations. Theor. Appl. Fract. Mech. 91, 76–85.
Giannella, V., Citarella, R., Perrella, M., Shlyannikov, V., 2019. Surface crack modelling in an engine compressor disc. Theor. Appl. Fract. Mech. 103, 102279. https://doi.org/10.1016/j.tafmec.2019.102279.
Grasso, M., Xu, Y., Russo, R., Rosiello, V., 2018. Mixed mode fatigue crack propagation behaviour of aluminium F357 alloy. Eng. Fail. Anal. 90, 463–475.
J. Hou, M. Goldstraw, S. Maan, and M. Knop, "An evaluation of 3D crack growth using ZENCRACK," 2001.
Kikuchi, M., Wada, Y., Ohdama, C., 2012. Effect of KIII on fatigue crack growth behavior. J. Eng. Mater. Technol. 134 (4), 041009.
Mi, Y., Aliabadi, M.H., 1994. Three-dimensional crack growth simulation using BEM. Comput. Struct. 52 (5), 871–878.

Nart, E., Ayhan, A.O., 2011. Crack insertion, meshing and fracture analysis of structures using tetrahedral finite elements. Eur. J. Mech. A/Solids 30 (3), 293–306.
Neves, A.C., Adey, R.A., Baynham, J.M.W., Niku, S.M., 1997. Automatic 3D crack growth using BEASY. WIT Trans. Modelling Simul. 19, 819–827.
Okada, H., Kawai, H., Tokuda, T., Fukui, Y., 2013. Fully automated mixed mode crack propagation analyses based on tetrahedral finite element and VCCM (virtual crack closure-integral method). Int. J. Fatigue 50, 33–39.
Paris, P., Erdogan, F., 1963. A critical analysis of crack propagation laws. J. Basic Eng. 85 (4), 528–533.
Pook, L.P., 1980. The significance of mode 1 branch cracks for combined mode failure. In: Radon, J.C. (Ed.), Fracture and Fatigue: Elasto-Plasticity, Thin Sheet And Micromechanism Problems. Pergamon Press, Oxford, pp. 143–153.
Pook, L., 1985. The fatigue crack direction and threshold behaviour of mild steel under mixed mode I and III loading. Int. J. Fatigue 7 (1), 21–30.
Richard, H.A., 2001. Experimental and numerical simulation of mixed-mode crack growth. In: Proceedings of the Sixth International Conference on Biaxial/Multiaxial Fatigue & Fracture, 2001, pp. 623–630.
Richard, H.A., Fulland, M., Buchholz, F.G., Schöllmann, M., 2003. 3D fracture criteria for structures with cracks. Steel Res. Int. 74 (8), 491–497.
Richard, H.A., Fulland, M., Sander, M., 2005. Theoretical crack path prediction. Fatigue Fract. Eng. Mater. Struct. 28 (1-2), 3–12.
Schöllmann, M., Richard, H.A., Kullmer, G., Fulland, M., 2002. A new criterion for the prediction of crack development in multiaxially loaded structures. Int. J. Fract. 117 (2), 129–141.
Schöllmann, M., Fulland, M., Richard, H.A., 2003. Development of a new software for adaptive crack growth simulations in 3D structures. Eng. Fract. Mech. 70 (2), 249–268.
Sih, G.C., 1991. A three-dimensional strain energy density factor theory of crack propagation. In: Sih, G.C. (Ed.), Mechanics of Fracture Initiation and Propagation. Springer Netherlands, Dordrecht, pp. 23–56. https://doi.org/10.1007/978-94-011-3734-8_2.
Tanaka, K., 1974. Fatigue crack propagation from a crack inclined to the cyclic tensile axis. Eng. Fract. Mech. 6 (3), 493–507.
Yaren, M.F., Demir, O., Ayhan, A.O., İriç, S., 2019. Three-dimensional mode-I/III fatigue crack propagation: computational modeling and experiments. Int. J. Fatigue 121, 124–134.
“ZENCRACK user manual, Issue 6.” Zentech Inc., 1999.